Surface & Coatings Technology 205 (2011) 4640–4648

Contents lists available at ScienceDirect

Surface & Coatings Technology

journal homepage: www.elsevier.com/locate/surfcoat

Comparative investigation of Al- and Cr-doped TiSiCN coatings

D.V. Shtansky [a,*], K.A. Kuptsov [a], Ph.V. Kiryukhantsev-Korneev [a], A.N. Sheveiko [a], A. Fernandez [b], M.I. Petrzhik [a]

[a] National University of Science and Technology "MISIS", Leninsky prospect 4, Moscow, Russia
[b] Instituto de Ciencia de Materiales de Sevilla, Centro Mixto CSIC-Universidad de Sevilla, Avda. Americo Vespucio 49, 41092-Sevilla, Spain

ARTICLE INFO

Article history:
Received 1 March 2011
Accepted in revised form 1 April 2011
Available online 9 April 2011

Keywords:
Al- and Cr-doped TiSiCN coatings
Magnetron sputtering
Structure
Mechanical and tribological properties
Thermal stability
High-temperature oxidation resistance

ABSTRACT

The aim of this work was a comparative investigation of the structure and properties of Al- and Cr-doped TiSiCN coatings deposited by magnetron sputtering of composite TiAlSiCN and TiCrSiCN targets produced by self-propagating high-temperature synthesis method. Based on X-ray diffraction, scanning and transmission electron microscopy, X-ray photoelectron spectroscopy, and Raman spectroscopy data, the Al- and Cr-doped TiSiCN coatings possessed nanocomposite structures (Ti,Al)(C,N)/a-(Si,C) and (Ti,Cr)(C,N)/a-SiC_xN_y/a-C with cubic crystallites embedded in an amorphous matrix. To evaluate the thermal stability and oxidation resistance, the coatings were annealed either in vacuum at 1000, 1100, 1200, and 1300 °C or in air at 1000 °C for 1 h. The results obtained show that the hardness of the Al-doped TiSiCN coatings increased from 41 to 46 GPa, reaching maximum at 1000 °C, and then slightly decreased to 38 GPa at 1300 °C. The Cr-doped TiSiCN coatings demonstrated high thermal stability up to 1100 °C with hardness above 34 GPa. Although both Al- and Cr-doped TiSiCN coatings possessed improved oxidation resistance up to 1000 °C, the TiAlSiCN coatings were more oxidation resistant than their TiCrSiCN counterparts. The TiCrSiCN coatings showed better tribological characteristics both at 25 and 700 °C and superior cutting performance compared with the TiAlSiCN coatings.

© 2011 Elsevier B.V. All rights reserved.

1. Introduction

Multicomponent coatings based on refractory transition metal carbides and nitrides attract a lot of attention as protective layers on the surface of cutting and stamping tools, as well as various mechanical components working under load-bearing conditions. Important coating properties for such applications are high hardness, wear, corrosion, and oxidation resistance, as well as low friction coefficient values.

The TiCN coatings succeeded the fist commercially available TiN and TiC coatings, combining the advantages of the high hardness of TiC and high ductility of TiN [1–3]. Silicon containing coatings are also increasingly used in surface engineering. Silicon nitride based ceramics are well known for their superior combination of fracture toughness and hardness, which are key properties for excellent wear resistance [4]. One of the most well-known examples of Si-doped coatings with extremely high hardness, thermal stability, and oxidation resistance is the nc-TiN/a-Si_3N_4 coatings developed by Vepřek et al. [5–7]. The hardness value of the TiSiCN coatings was found to vary from 25 to 55 GPa [8–12] and the coatings maintained their high hardness up to 800–850 °C [9,11]. It has been shown that, in addition to high hardness, the Si-doped TiCN coatings are characterized by superior wear, oxidation, and corrosion resistance [8,9]. The TiSiCN coatings with low friction coefficient values were also reported [12–15].

High thermal stability and oxidation resistance are critical properties for protective coatings working at elevated temperatures. Further improvement in high-temperature properties of multicomponent coatings can be achieved by a proper choice of additional alloying elements such as Al or Cr [16]. It is known that Al and Cr have a positive effect on the thermal stability and oxidation resistance of titanium carbides, borides, and nitrides and improve their wear resistance, especially at high temperatures [17–19]. For instance, the Al-doped TiCN and TiCrCN coatings showed superior thermal stability since their cubic structure was stable in the temperature range of 25–1200 °C [20]. The Cr incorporation was also shown to significantly improve the thermal stability, corrosion, and high-temperature oxidation resistance of TiBN coatings [21].

To the best of our knowledge, Al- and Cr-doped TiSiCN coatings were not investigated. Thus the aim of this work was a comparative investigation of the structure and properties of Al- and Cr-doped TiSiCN coatings deposited by magnetron sputtering of composite TiAlSiCN and TiCrSiCN targets produced by self-propagating high-temperature synthesis (SHS) method. In addition, the lifetimes of cutting tools coated with TiAlSiCN and TiCrSiCN coatings in dry

* Corresponding author. Tel.: +7 499 236 6629; fax: +7 499 236 5298.
E-mail address: shtansky@shs.misis.ru (D.V. Shtansky).

0257-8972/$ – see front matter © 2011 Elsevier B.V. All rights reserved.
doi:10.1016/j.surfcoat.2011.04.012

milling of D2 steel were compared with those of uncoated tools and tools coated with TiN reference film.

2. Materials and methods

The TiAlSiCN and TiCrSiCN targets were synthesized from various exothermal mixtures using the combined force SHS-pressing technology, as described elsewhere [22]. The synthesized targets, 120 mm in diameter and 6–8 mm thick, were magnetron sputtered in a gaseous mixture of argon and nitrogen at a nitrogen partial pressure $N_2/(N_2+Ar)$ of 14%. The applied magnetron current and voltage were 2 A and 500 V, respectively. During deposition, the total pressure was maintained at 0.1 Pa, the bias voltage was −50 V, and the substrate temperature was kept constant at 300 °C (TiCrSiCN coatings). Preliminary investigations showed that the TiAlSiCN coatings deposited at the substrate temperature below 500 °C had poor mechanical properties, therefore in the present study the deposition experiments with TiAlSiCN coatings were fulfilled at 500 °C. Single crystal Si(100), cemented carbide (WC + 6%Co), Ni foil (H-2), and Al_2O_3 were used as substrates. All substrates were ultrasonically cleaned in isopropyl alcohol for 5 min and etched by Ar ions directly in the vacuum chamber for 5–10 min prior to deposition. To enhance coating adhesion to substrates, high-energy ion bombardment with average Ti^{2+} ion energy of about 70 keV was applied for 10 min at the beginning of deposition. The accelerating voltage, ion current, and ion flux were kept constant at 35 kV, 10 mA, and 2×10^{14} ions $cm^{-2}\,s^{-1}$, respectively.

The as-deposited coatings were annealed either in vacuum at 1000, 1100, 1200, and 1300 °C or in air at 1000 °C for 1 h. The residual pressure during vacuum annealing was below 10^{-3} Pa. The thermal stability of coatings was evaluated by means of structural investigation and load-depth-sensing nanoindentation measurements prior to and after annealing. The elemental depth profiles for the oxidized films were obtained by glow discharge optical emission spectroscopy (GDOES) using a PROFILER-2 instrument (Horiba Jobin Yvon).

The structure, elemental and phase composition of coatings were studied by means of X-ray diffraction (XRD), scanning and transmission electron microscopy (SEM and TEM), X-ray photoelectron spectroscopy (XPS), Raman spectroscopy, and GDOES as described elsewhere [20]. The XRD investigations were performed with coatings deposited on Si (100), cemented carbide, and alumina substrates. The XRD patterns for coatings deposited on cemented carbide and alumina substrates were recorded on a D8 Advance X-ray diffractometer (Bruker) using a CuK_α radiation. In the case of the coatings deposited on Si (100) substrates, a "Geigerflex" X-ray diffractometer was used with a CoK_α radiation. The microstructure of the coatings was examined by a transmission JEM-200CX and scanning JSM-6700F electron microscopes (both JEOL, Japan) operating at 200 kV and 15 kV, respectively. For TEM studies samples with coatings deposited on 200 μm thick Ni substrates were prepared from 3-mm disks, ground to a thickness of about 0.05 mm from the substrate side, and electropolished by a one-side polishing method using an electrolyte containing H_3PO_4 and Cr_2O_3. A Leybold Heraus ESCALAB 210 spectrometer was used to obtain XPS spectra. The base pressure in the XPS ion cleaning chamber and analysis chamber was $(2.66–4.0)\times10^{-6}$ Pa and 1.33×10^{-7} Pa, respectively. XPS spectra were recorded after removing surface contaminations by Ar^+ ion etching. The elemental compositions of the as-deposited coatings were determined using GDOES elemental profiles. A typical set of standard samples from Horiba Jobin Yvon and TiCN-based coatings with well known elemental composition obtained by XPS were used for calibration. The Raman spectra were excited by a 514 nm laser radiation and recorded using a LABRAM HR 800 (Horiba Jobin Yvon) spectrometer with a resolution of 1 cm^{-1}.

The measurements of hardness, *H*, and elastic modulus, *E*, were performed by load-depth-sensing nanoindentation method using a Nano Hardness Tester (CSM Instruments) equipped with a Berkovich diamond indenter tip calibrated against fused silica.

The tribological properties of the coatings deposited on cemented carbide substrates were evaluated at an ambient temperature of 25 °C using a pin-on-disk tribometer (CSM Instruments) under a normal load of 5 N and a sliding speed of 0.1 m/s. A WC + Co ball, 3-mm in diameter, was chosen as a counterpart material. The high-temperature tribological experiments were performed for coatings deposited on Al_2O_3 substrates at 700 °C using a high-temperature pin-on-disc tribometer (CSM Instruments). The tests were carried out under a normal load of 1 N with an Al_2O_3 ball, 6-mm in diameter, as a counterpart material.

The milling tests were carried out on a drill-milling machine VF-1 (HAAS, USA) under a rotation speed of 1900 rpm, a feeding rate of 150 mm/min, and an allowance of 0.2 mm. Coated and uncoated 8 mm diameter WC-Co end mills (SGS Tool Co., USA) were used in dry milling of D2 steel (Cr12MoV, 53 HRC).

3. Results and discussion

3.1. Composition and structure

The SEM fracture cross-sections of the Cr- and Al-doped TiSiCN coatings are shown in Fig. 1. The TiCrSiCN coating deposited at 300 °C revealed a fine columnar structure with a column width in the range of 50–150 nm (Fig. 1a). As revealed by the dark-field (DF) TEM micrograph, the coating was characterized by a crystallite size ranging from 8 to 20 nm (Fig. 2a). Thus the crystallite size was smaller than the column width. The average crystallite size determined from the (111) and (200) XRD peaks at their full width at half maximum (FWHM) using the Scherrer formula was 4 nm, that is smaller than the lower limit of particle size range determined from DF TEM. Therefore additional factors, such as the presence of defects and inhomogeneous strain, contribute to the peak widths. The TiAlSiCN

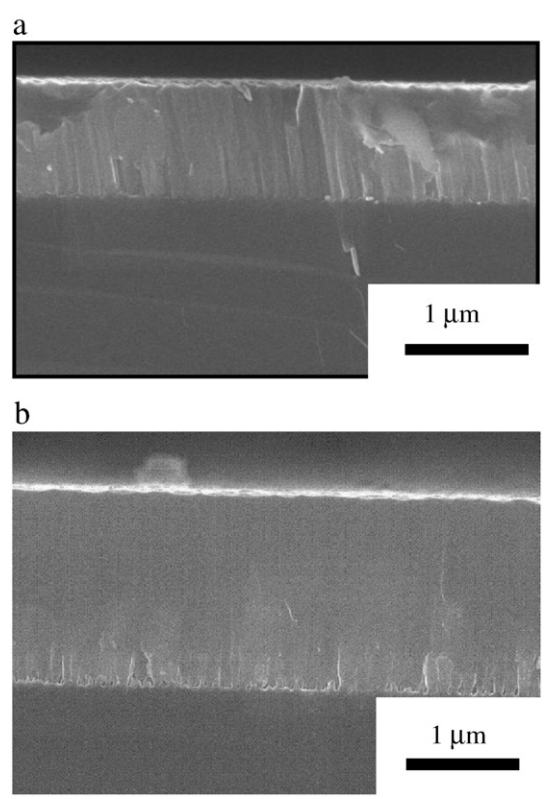

Fig. 1. Typical SEM cross-sectional fracture micrographs of the as-deposited (a) TiCrSiCN and (b) TiAlSiCN coatings deposited on Si substrates.

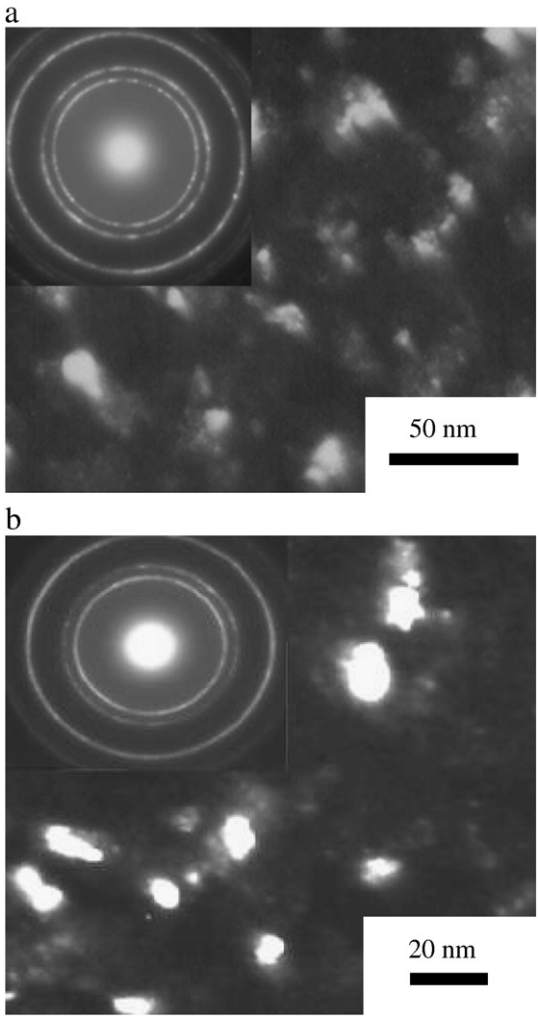

Fig. 2. Dark-field TEM micrographs (plan-view) of the (a) TiCrSiCN and (b) TiAlSiCN coatings.

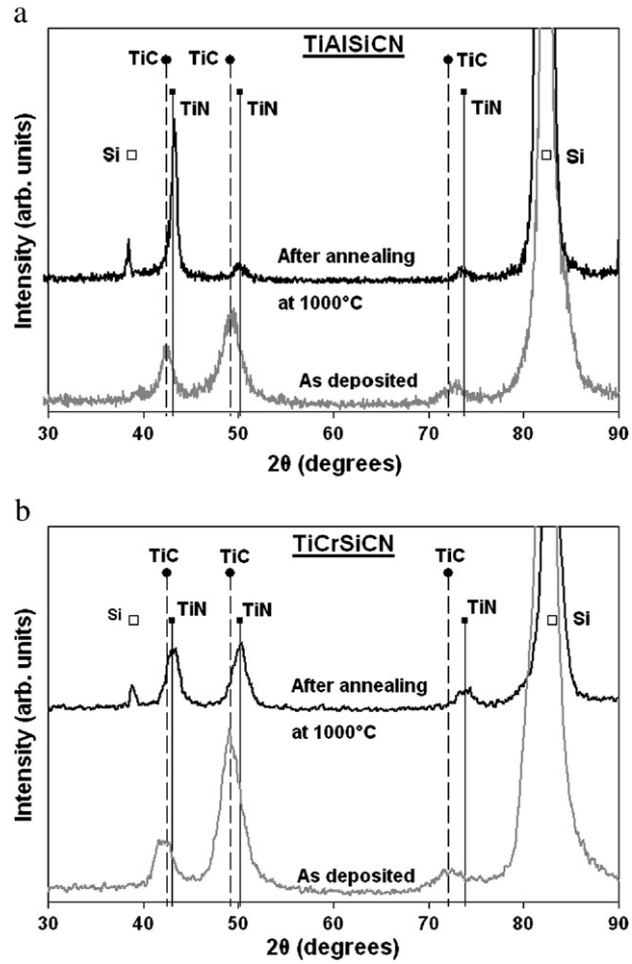

Fig. 3. XRD patterns of (a) TiAlSiCN and (b) TiCrSiCN coatings. XRD patterns of (a) TiAlSiCN and (b) TiCrSiCN coatings. The reference marks for the Si substrate and reference lines for TiC (ICDD card no. 02–1179), and TiN (ICDD card no. 87–0632) are also shown.

coating deposited at 500 °C exhibited a two-layer structure (Fig. 1b). The top layer reveals an extremely dense, homogeneous and featureless morphology. The underlayer with a columnar structure observed at the coating/substrate interface was deposited by ion implantation assisted magnetron sputtering at the very beginning of deposition process. The formation of intermediate layers at the coating/substrate interface was previously reported for coatings deposited by ion implantation assisted magnetron sputtering [23] and can be attributed to high-energy ion bombardment which affected the coating growth conditions. When ion implantation is used, the energy delivered to the coating during its growth increases. This enhances the surface mobility of adatoms, leading to the formation of columnar structure. As determined from the DF TEM micrograph (Fig. 2b), the crystallite size of the TiAlSiCN top layer ranged from 3 to 15 nm, which agrees well with XRD results, 6 nm. The thorough structural characterization using XRD (Fig. 3) and selected area electron diffraction (SAED) patterns (Fig. 2, insets) identified all the TiCrSiCN and TiAlSiCN coatings as having a cubic B1 NaCl-type structure without any preferential orientation. Note that the XRD spectra of coatings deposited on Si and WC-Co substrates were similar.

Additional information about the coating structures can be obtained by analyzing the corresponding XPS spectra. Typical Ti 2p, N 1s, C 1s, Si 2p, Cr 2p, and Al 2p XPS spectra of the TiCrSiCN and TiAlSiCN coatings are presented in Fig. 4a–f. The Ti 2p XPS spectrum of the TiCrSiCN coating (Fig. 4a) had the main peaks at 455.2 and 461.0 eV, which match the TiC and TiN phases [24,25]. The Ti $2p_{3/2}$ and $2p_{1/2}$ peaks in Fig. 4a have a broad asymmetrical shape with a low slope on the high-energy side that can be attributed to an oxidized TiCNO state [26]. The existence of the Ti–N and Ti–C bonds in the TiCrSiCN coating is also evident from the presence of characteristic N 1s and C 1s bands at 397 and 281.4 eV, respectively (Fig. 4b and c) [27]. Moreover, the shoulder of the C 1s peak at higher binding energies gives evidence for the presence of at least two forms of carbon: metallic carbonitride (283 eV) [28] and free amorphous or graphitic carbon (284.5 eV) [29]. The Si 2p spectrum (Fig. 4d) shows a characteristic band at 101 eV, just between 100.45 eV (SiC phase [30]) and 101.8 eV (Si_3N_4 phase [27]). The Cr $2p_{3/2}$ peak at 574.6 eV (Fig. 4e) is close to that of chromium carbonitride [28] but considerably broader due to the presence of Cr in nitride or oxide states [29,31,32]. Summarizing the XPS data, it can be concluded that the TiCrSiCN coatings consisted of (Ti,Cr)(C,N) as a main phase with a certain amount of additional phases based on SiC_xN_y and carbon. Since these additional phases were not detected by XRD and SEAD techniques, they are believed to be in amorphous state at the grain boundaries of the cubic phase.

The Ti 2p and N 1s peaks of the TiAlSiCN coating are shifted by 1 and 1.3 eV, respectively, to lower binding energies from the peak positions of the TiCrSiCN coating (Fig. 4a and b). In addition, the Al 2p spectrum of the TiAlSiCN coating (Fig. 4f) shows a characteristic band at 73.1 eV, which is higher than 72.8 eV for metallic Al 2p but lower than 74.5 eV for Al 2p in AlN [33]. The observed positions of binding

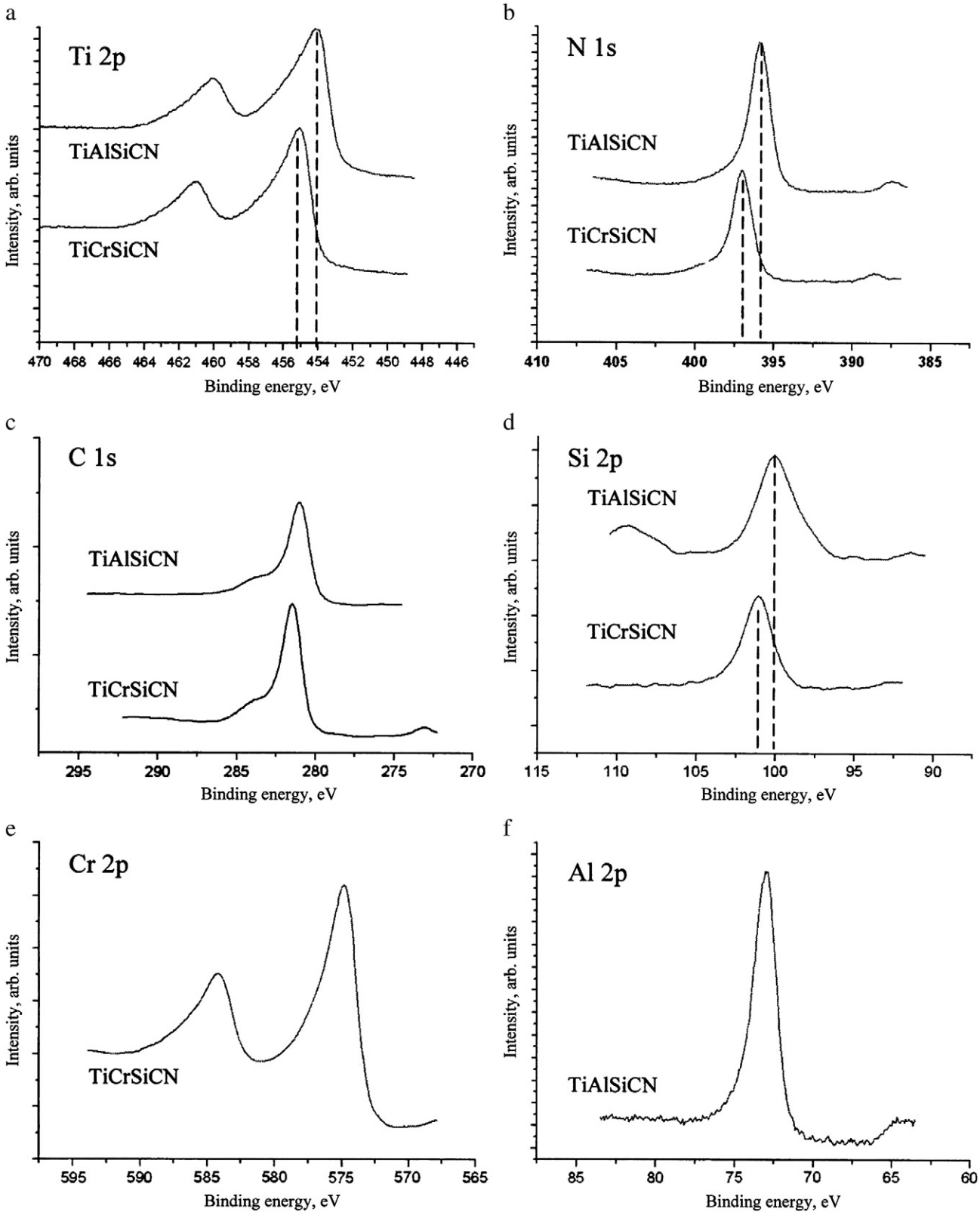

Fig. 4. XPS spectra of the TiCrSiCN and TiAlSiCN coatings.

energies may be attributed to the formation of a nonstoichiometric $(Ti,Al)(C,N)_x$ phase. In the Si 2p spectrum of the TiAlSiCN coating (Fig. 4d), the peak at the binding energy of 100 eV is due to metallic silicon, which is probably in an amorphous state, or Si-doped DLC, which has a peak at 100.5 eV [34].

The Raman spectra of the as-deposited coatings are shown in Fig. 5. The spectrum of the TiCrSiCN coating represents two broad bands centered at 236 (TA) and 552 cm^{-1} (TO) which are characteristics of TiN [35] or C-doped TiN [36]. For the TiAlSiCN coating, the acoustic (TA) peak is shifted to a higher wave-number position at

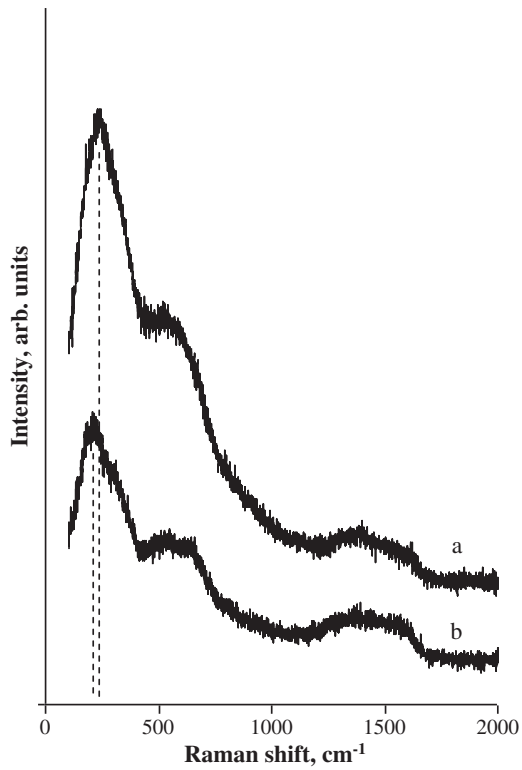

Fig. 5. Raman spectra of the (a) TiAlSiCN and (b) TiCrSiCN coatings.

276 cm^{-1} (Fig. 5), which is in agreement with the TiCN phase [37]. This indicates a higher carbon content in the TiCN compound of the TiAlSiCN coating compared with the TiCrSiCN coating. The band intensity ratio depends on the nitrogen and carbon contents in the TiCN phase. The first-order scattering was shown to become more pronounced when the deviation from the stoichiometry was increased [38]. For both spectra in Fig. 5 the intensity of the acoustic mode was seen to be higher than that of the optic mode. This is due to a high density of defects as a result of deficiency of nonmetallic atoms in the cubic sublattice [35]. Thus in both coatings the cubic phase was nonstoichiometric, which agrees well with XPS results. The spectra also show very broad peaks of diamond-like or amorphous carbon located between 1180 and 1680 cm^{-1}.

Summarizing the XRD, SAED, XPS and Raman spectroscopy data, it can be concluded that the TiCrSiCN coatings consisted of (Ti,Cr)(C,N) as a main phase with a certain amount of amorphous SiC_xN_y and a-C phases. At the same time, in addition to the main (Ti,Al)(C,N) phase, the TiAlSiCN coatings contained some amount of the a-(Si,C) phase. The elemental compositions of the TiCrSiCN and TiAlSiCN coatings were determined from GDOES analysis and are shown in Table 1. It can be seen that the elemental and phase compositions of the coatings are in a good agreement.

3.2. Tribological characteristics

The TiCrSiCN coatings tested at room temperature against a 3 mm WC + Co ball showed a stable friction coefficient within the range of 0.4–0.45 without any initial maximum. The friction coefficient of the TiAlSiCN coatings displayed an initial maximum of 0.6 followed by a drop to 0.5 after a short run-in period of 30 m and a further gradual increase to 0.7 after a 300 m pass. The wear rate of the TiCrSiCN and TiAlSiCN coatings was 1.5×10^{-6} and 6.0×10^{-6} $mm^3\,N^{-1}\,m^{-1}$, respectively.

Fig. 6a and b shows the friction coefficients of the TiCrSiCN and TiAlSiCN coatings deposited on Al_2O_3 substrates against a 6 mm Al_2O_3 ball. For Al-doped coatings tested at 25 and 700 °C, the friction coefficient values in the range of 0.9–1.0 were recorded. The wear mechanism changed from abrasive to adhesion wear with increasing temperature from 25 to 700 °C (Fig. 6c, curves 3 and 4). As shown below, the TiAlSiCN coatings had a very high oxidation resistance, which is why the intensive oxidation of the coatings during the tribological test at 700 °C was not expected. As a result, the wear rate of the TiAlSiCN coatings decreased from 5.5×10^{-5} to 2.5×10^{-5} $mm^3\,N^{-1}\,m^{-1}$ whereas that of the Al_2O_3 ball increased form 0.6×10^{-6} to 9.5×10^{-6} $mm^3\,N^{-1}\,m^{-1}$. For the Cr-doped coatings, the steady-state friction coefficient value increased from 0.45 to 0.8 when the test temperature was raised from 25 to 700 °C (Fig. 6a and b). The analysis of the wear tracks indicated that the TiCrSiCN coatings exhibited adhesive wear independent on the environment temperature (Fig. 6c, curves 1 and 2). In contrast to the TiAlSiCN coatings, the wear rates of both the TiCrSiCN coating and Al_2O_3 ball increased with temperature from 3.7×10^{-6} and 0.1×10^{-6} $mm^3\,N^{-1}\,m^{-1}$ to 4.3×10^{-5} and 5.5×10^{-6} $mm^3\,N^{-1}\,m^{-1}$, respectively.

3.3. Thermal stability

Fig. 3 compares the XRD patterns of the TiCrSiCN and TiAlSiCN coatings deposited on Si substrate and annealed in vacuum at 1000 °C for 1 h with those of the as-deposited coatings. It can be seen that at the annealing temperature of 1000 °C, the preferential orientation of the TiCrSiCN coating slightly changed due to the increase of a number of grains with (111) orientation at the expense of (200) grains and the crystallite size slightly increased from 4 to 6–7 nm, as determined from the XRD (111) and (200) peak widths using the Scherrer formula. In the TiAlSiCN coating the texture changed from (100) to (111) and the crystallite size increased from 6 to 12 nm (Fig. 3b).

For annealing experiments at 1200 °C, cemented carbide substrates were used because single crystal Si undergoes phase transformation, which makes the analysis of XRD patterns complicated. In the case of the TiCrSiCN coatings, no significant phase change was observed in the XRD pattern after heat treatment at 1200 °C for 1 h (Fig. 7) if compared to patterns in Fig. 3. The (200) and (220) peaks reveal strong asymmetrical maxima close to the positions of TiC and TiN reference lines with a shoulder on the high-angle side, suggesting a short-range redistribution of elements between neighbor phases during annealing and separation in two cubic phases with different lattice parameters, which are believed to be Cr-rich and Cr-deficient. During annealing of the TiAlSiCN coatings at 1200 °C, the phase separation started with a precipitation of *h*-AlN phase (Fig. 7). We also observed cobalt droplets on the surface of the TiAlSiCN coatings due to the diffusion of metal atoms from WC-Co substrate into the coating. The precipitation of the *h*-AlN phase was often observed in the TiAlCN system at high temperatures between 800 and 1000 °C [20,39]. In a number of systems, such as TiAlCN, TiCrAlCN, and TiCrAlSiN, the *h*-AlN phase was

Table 1
Compositions of as-deposited coatings.

Coating	Target green mixture, wt.%	Elemental composition of coating, at.%						Phase composition of coating
		Ti	Al	Cr	Si	C	N	
TiAlSiCN	Ti + 17.3Al + 14.3Si_3N_4 + 4.5C	31.8	15.1	–	7.0	19.5	26.6	$(Ti,Al)(C,N)_x$, a-(Si,C)
TiCrSiCN	Ti + 25.1Cr + 11.9Si_3N_4 + 7.2C	26.0	–	17.0	7.0	28.0	22.0	$(Ti,Cr)(C,N)_x$, SiC_xN_y, a-C

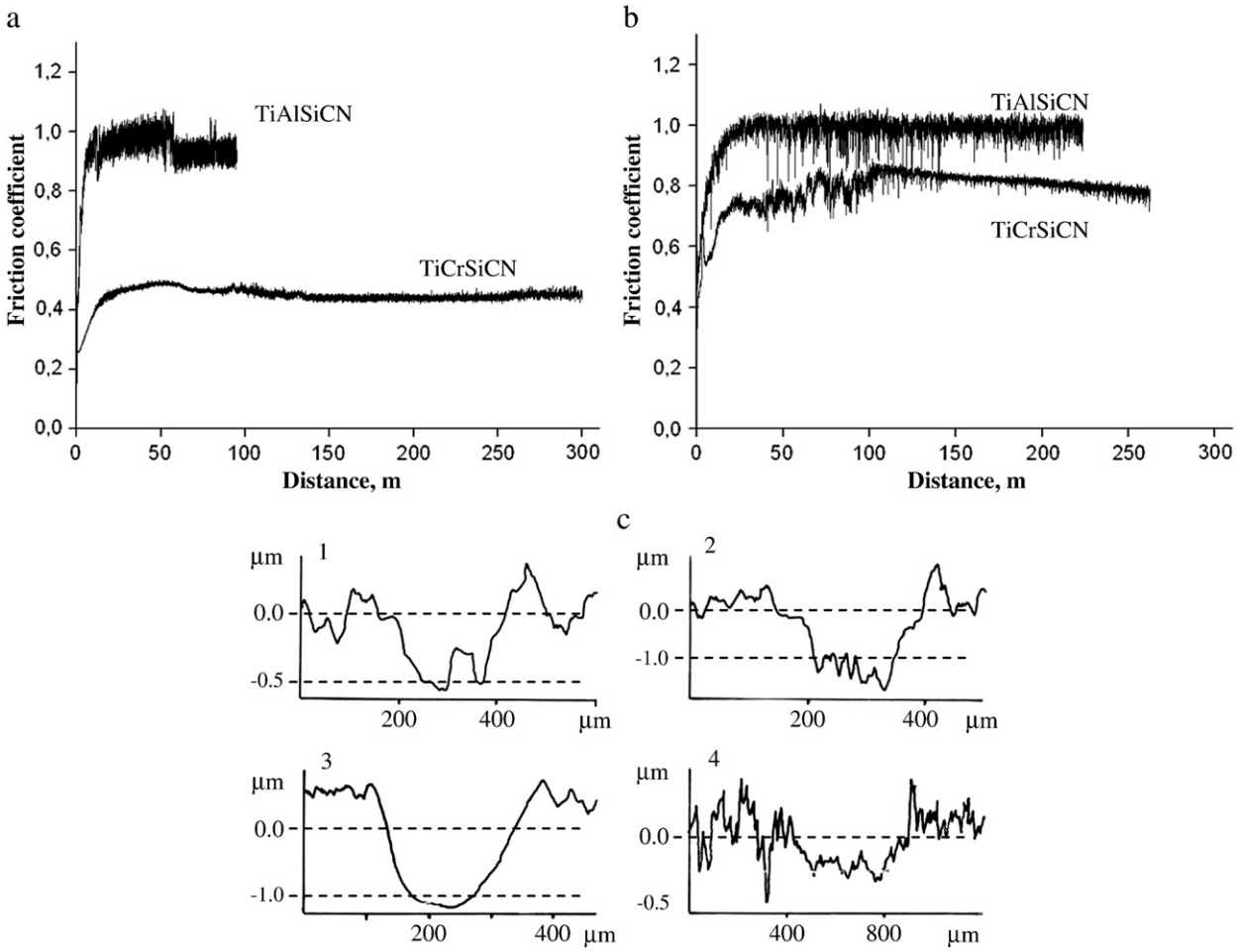

Fig. 6. Friction coefficients of the TiCrSiCN and TiAlSiCN coatings as a function of running distance. (a) 25 °C; (b) 700 °C. (c) Profiles of the vertical cross section of the wear tracks: 1 — TiCrSiCN, 25 °C; 2 — TiCrSiCN, 700 °C; 3 — TiAlSiCN, 25 °C; and 4 — TiAlSiCN, 700 °C.

reported to completely disappear with further increase in temperature up to 1200 °C. This phenomenon was not completely understood because the *h*-AlN phase is the most stable phase in the ternary TiAlN system [20,40]. One of the explanations could be the influence of Co atoms which diffused outward to the surface and changed the coarsening mechanism. Veprek et al. reported that the precipitation of the *h*-AlN phase was not observed in the nc-(Al,Ti)N/a-Si_3N_4 coatings even after vacuum annealing at 1100 °C due to an immiscible Si_3N_4 tissue which covered (Al,Ti)N nanograins [41]. The addition of silicon was shown to delay the appearance of h-AlN phase and thereby improved the thermal stability of the coatings [42]. These results were also confirmed in the present study. Thus the onset of precipitation and dissolution of h-AlN phase depends to a great extent on the type of structure, elemental and phase composition of multicomponent coatings.

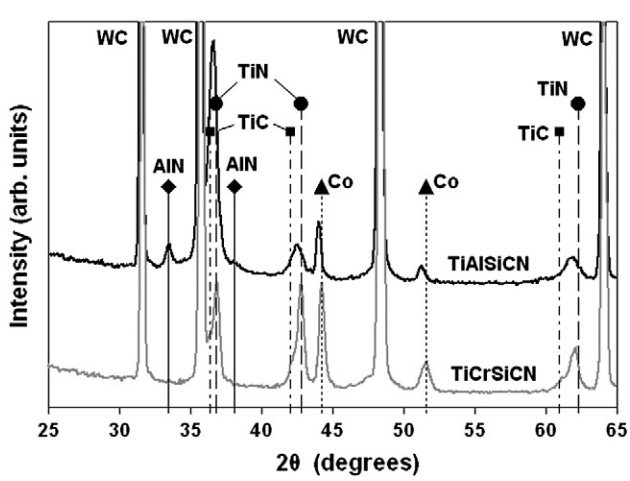

Fig. 7. XRD patterns of the TiAlSiCN and TiCrSiCN coatings deposited on cemented carbide substrates after annealing in vacuum at 1200 °C for 1 h. The reference lines for the WC + Co substrate, AlN (ICDD card No. 79–2497), TiC (ICDD card No. 02–1179), and TiN (ICDD card No. 87–0632) are also shown.

Coatings with a cubic structure usually show good diffusion barrier properties for metal atom diffusion from the substrate toward the surface [19]. As was shown above, the TiAlSiCN coatings were not stable enough at 1200 °C and were subjected to a phase transformation due to cobalt diffusion. In the case of the TiCrSiCN coatings subjected to a heat treatment at 1200 °C, we observed neither phase transformations nor any precipitation of cobalt droplets on the coating surface, which suggests high diffusion barrier characteristics of the coatings.

In order to avoid the influence of substrate material on the coating thermal stability, further experiments were fulfilled with Al_2O_3 substrates. Fig. 8a compares the shape and position of the (111) peak of the as-deposited TiCrSiCN coating with those after annealing in vacuum at 1000 and 1200 °C. For coatings deposited on Al_2O_3 substrates, several special features should be mentioned. Firstly, the as-deposited TiCrSiCN coatings showed a strong (111) preferential orientation while no other peaks from the cubic phase were observed. The broad asymmetrical shape of the peak observed in the pattern of the as-deposited TiCrSiCN coating can be explained by the

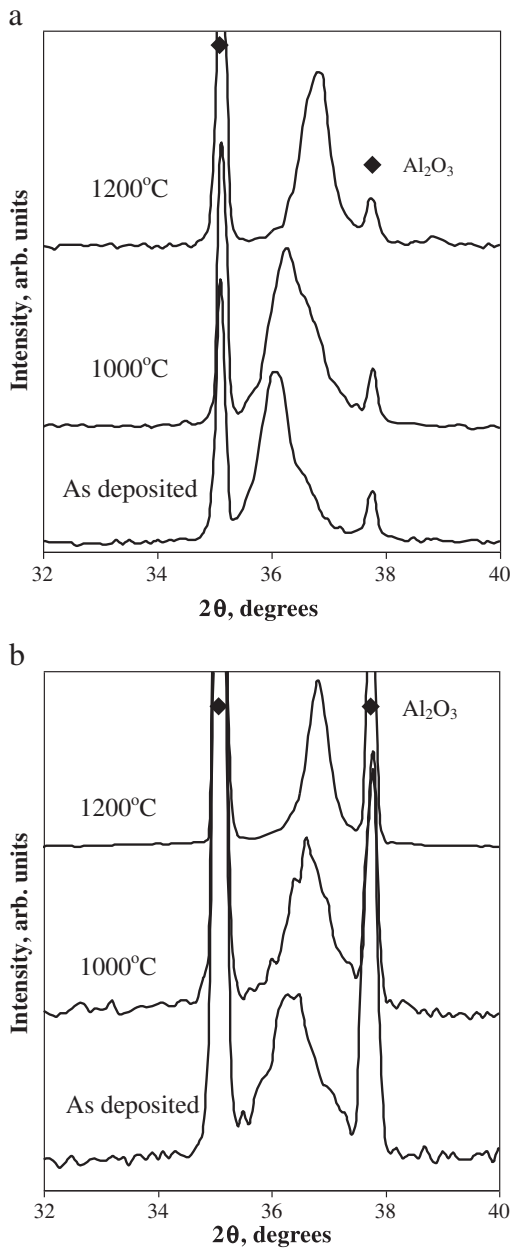

Fig. 8. Evolution of XRD patterns of the (a) TiCrSiCN and (b) TiAlSiCN coatings during annealing in vacuum.

superposition of reflections from (111) planes of two fcc phases with various compositions, which are probably rich and poor in Cr. This structure is quite stable because a similar shape of the (111) peak was observed after annealing at 1000 °C. Secondly, the average grain size, as determined from the FWHM of the (111) XRD peak, was 15 nm, which is higher than that of 4 nm for the TiCrSiCN coating deposited on cemented carbide substrate under similar deposition conditions. Thirdly, the coating showed a very high thermal stability; the grain size did not change in the temperature range of 25–1200 °C being of about 15 nm (Fig. 8a). The shift observed in the position of the (111) peaks could be attributed to a short-range diffusion and element redistribution between the neighbor grains without any phase transformation or grain growth. As a result, the lattice parameter of the cubic phase decreased from the value of 0.249 nm, typical for TiC, to 0.244 nm, which is characteristic of TiN.

The XRD patterns for the TiAlSiCN coatings are presented in Fig. 8b. Upon annealing up to 1000 °C, the grain size remained almost constant in the range of 9–11 nm whereas the lattice parameter decreased from 0.247 to 0.245 nm. After heat treatment at 1200 °C, the lattice parameter further decreased to 0.243 nm and the grain size increased up to 19 nm. Note that the precipitation of the h-AlN phase, which has the (100) peak at $2\theta = 33.2°$, was not observed even after annealing at 1200 °C. Thus the addition of silicon to TiAlCN coatings postponed the decomposition of fcc phase by 200–400 °C.

Fig. 9 shows the hardness of the TiCrSiCN and TiAlSiCN coatings deposited on Al_2O_3 substrates as a function of annealing vacuum temperature. The TiCrSiCN coatings showed a small decrease in hardness from 37 to 34 GPa between 25 and 1100 °C. It is in agreement with the XRD results that no substantial structural changes were observed after annealing at 1000 °C except a slight decrease in the lattice parameter. With further increase in temperature up to 1200 °C, the hardness decreased to 27 GPa being still high enough for many high-temperature tribological applications. The hardness of the TiAlSiCN coatings increased from 41 to 46 GPa at 1000 °C, after which it continuously decreased to 41 GPa at 1200 °C and 37 GPa at 1300 °C. Thus the TiAlSiCN coatings showed a high hardness over 37 GPa in a very broad temperature range of 25–1300 °C. This hardness is considerably higher than 27 GPa reported for the nc-(Al,Ti)N/a-Si_3N_4 coatings after annealing at 1250 °C [41]. It should be noted that high values of post-annealing hardness observed for TiAlCN coatings up to 1200 °C were previously reported but they did not exceed 32 GPa [20]. The gradual decrease of hardness for the TiAlSiCN coatings at temperatures above 1100 °C can be attributed to the small increase in the grain size.

3.4. Oxidation resistance

The oxidation profiles of the coatings after annealing at 1000 °C for 1 h were determined using GDOES (Fig. 10). The TiAlSiCN and TiCrSiCN coatings, 2.7 μm thick, were only partly oxidized with oxidation depths of 0.7 and 1.1 μm, respectively. At somewhat lower oxidation temperatures, the oxidation depth difference between the Al- and Cr-doped coatings was lower, being 150 and 220 nm at 800 °C and 470 and 590 nm at 900 °C, respectively. Fig. 10 also shows that a titanium oxide film was formed on the outmost surface of the coatings. The TiO_2 film was followed by a thin CrO_x (Cr-doped coating) or Al_2O_3 (Al-doped coating) layers which protect the coatings from further oxidation. Note that in the case of the TiAlSiCN coatings, the oxidation structure was more complicated. The formation of the TiO_x and SiC layers was observed just beneath the alumina film (Fig. 10b). It should be also mentioned that, among other

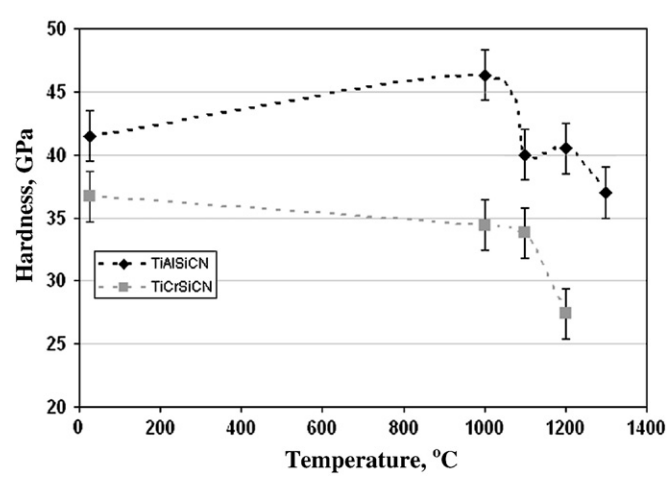

Fig. 9. Hardness of the Al- and Cr-doped TiSiCN coatings as a function of annealing temperature in vacuum. Values at 25 °C are those for the as-deposited coatings. Lines are only used as guides to the eye.

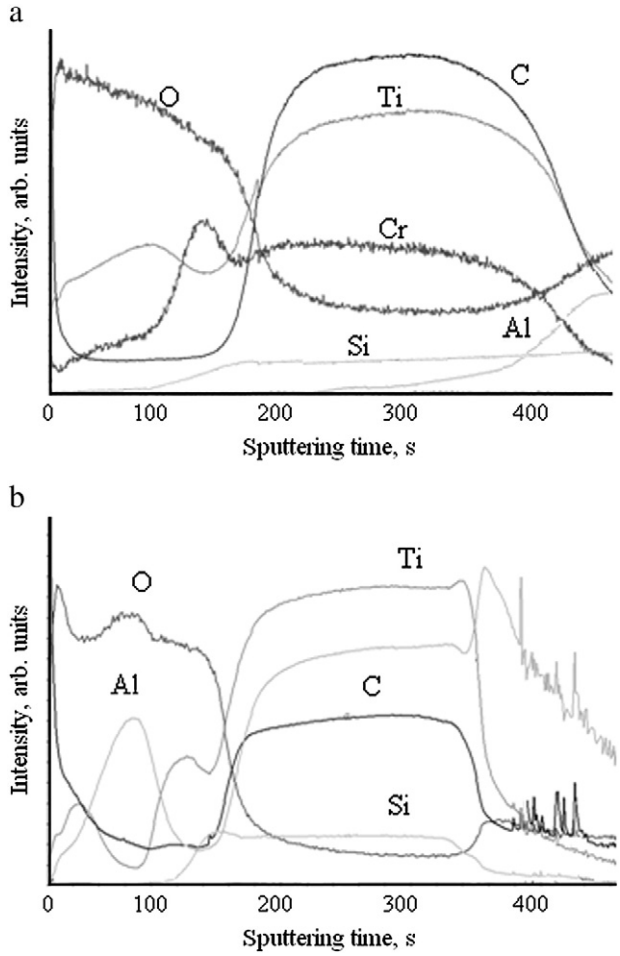

Fig. 10. GDOES depth profiles of the (a) TiCrSiCN and (b) TiAlSiCN coatings after oxidation in air at 1000 °C for 1 h.

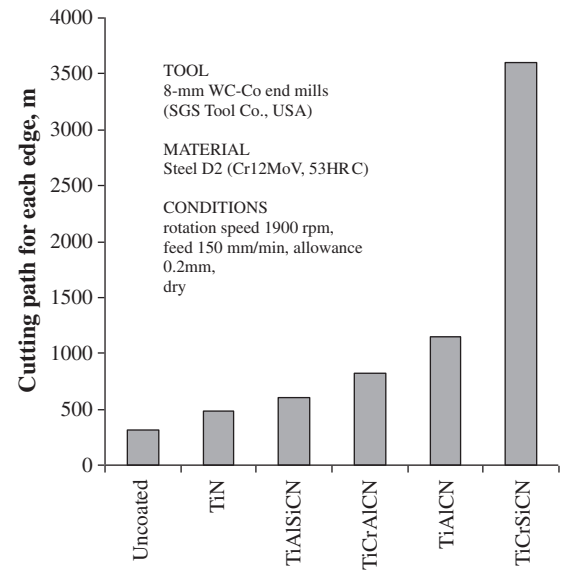

Fig. 11. Comparison of lifetime of coated and uncoated tools in dry milling operations.

parameters, the oxidation of the coatings is controlled by microporosity, which is somewhat higher for the TiCrSiCN coatings due to a columnar structure.

3.5. Cutting tests

Comparison of lifetimes of coated and uncoated 8 mm diameter WC-Co end mills (SGS Tool Company, USA) in dry milling of high-chromium steel (X12BF brand mark, 52–53 HRC) is shown in Fig. 11. The performance of the TiAlSiCN and TiCrSiCN coatings was compared with that of uncoated tools and tools coated with TiN, TiAlCN, and TiCrAlCN films [20]. It can be seen that the TiCrSiCN coatings demonstrate superior cutting performance. The lifetimes of end mills with TiCrSiCN coatings were three times longer compared to their counterparts with TiAlCN and TiAlSiCN coatings. This superior cutting performance of the Cr-doped coatings can be attributed to lower values of friction coefficient both at ambient and elevated temperatures compared with Al-doped coatings.

Based on the literature data, high hardness and oxidation resistance are the key properties for durable tools with long lifetime. For instance, the superior performance of the TiCrAlN coatings compared with TiAlN coatings was attributed to their increased hardness and oxidation resistance [43]. Fox-Rabinovich and co-workers [44] reported that the TiAlCrN coatings with the best oxidation stability at elevated temperatures had the longest cutting tool life. The coating friction coefficient is another important parameter. Low friction coefficient implies both decreased friction between the tool and chip in dry machining and reduced tendency to sticking and material pick up from the counterpart material, which leads to the extended service life of cutting tools. The latter statement is supported by a number of studies. The superior milling performance of the TiAlCN coatings compared to the CrAlCN coatings was attributed to its better mechanical (high hardness) and tribological (low friction) properties [20]. Imamura et al. [45] also reported that the TiSiCN coatings outperformed the TiAlN and TiSiN coatings in milling tests due to their better tribological properties. The hardness of the TiAlSiCN coatings reported in the present work is higher compared with that of the TiCrSiCN coatings and the difference is even larger at high temperatures. Both coatings showed only minor oxidation at 800 °C. Since the operating temperatures during our milling experiments did not appear to exceed 800 °C, both TiAlSiCN and TiAlSiCN coatings had sufficiently high hardness and oxidation resistance for good cutting performance under such circumstances. This is in good agreement with the above conclusion that low friction and wear ensure the superior cutting performance of the Cr-doped coatings.

4. Summary

The TiAlSiCN and TiCrSiCN coatings were prepared by magnetron sputtering of composite targets and characterized as hard, wear resistant materials for high-temperature tribological applications. The most important results can be summarized as follows.

The TiCrSiCN coatings consisted of (Ti,Cr)(C,N) as a main phase with a certain amount of amorphous SiC_xN_y and a-C phases. In the TiAlSiCN coatings, apart from the (Ti,Al)(C,N) phase, the indications of amorphous Si and C were observed.

The TiCrSiCN coatings exhibited adhesive wear independent on the environmental temperature, whereas the wear mechanism of the TiAlSiCN coatings changed from abrasive to adhesion wear with increasing temperature from 25 to 700 °C. The tribological properties of the Cr-doped TiSiCN coatings were superior to the Al-doped TiSiCN coatings both at 25 and 700 °C.

The TiAlSiCN coatings showed the high hardness above 37 GPa in a very broad range of temperature from 25 to 1300 °C. The TiCrSiCN coatings demonstrated the hardness above 34 GPa up to 1100 °C, but then the hardness dropped to 27 GPa at 1200 °C. The TiAlSiCN coatings were more oxidation resistant than the TiCrSiCN coatings. After being exposed to air for 1 h at 1000 °C, the TiCrSiCN and TiAlSiCN

coatings, both 2.7 μm thick, were only partly oxidized, with oxidation depths of 0.7 (TiAlSiCN) and 1.1 μm (TiCrSiCN).

The end mills with Cr-doped TiSiCN coatings showed superior dry cutting performance against a high-chromium steel compared to the Al-doped TiSiCN coatings and reference TiAlCN and TiAlCrCN coatings. This can be attributed to their better tribological properties (low friction and wear).

Acknowledgment

The work was fulfilled due to financial support from the Ministry of Education and Science of the Russian Federation (Contracts 02.740.11.0859 and П1248). The authors thank A.V. Levanov (Moscow State University) for Raman spectroscopy investigations and T.B. Sagalova (MISIS) for help with XRD measurements.

References

[1] H. Randhawa, Thin Solid Films 153 (1987) 2009.
[2] E. Damond, P. Jacquot, Mater. Sci. Eng. A 140 (1991) 838.
[3] L. Karlsson, L. Hultman, M.P. Johansson, J.-E. Sundgren, H. Ljungcrantz, Surf. Coat. Technol. 126 (2000) 1.
[4] G. Petzow, M. Herrmann, in: M. Janson (Ed.), High Performance Non-Oxide Ceramics II, Structure and Bonding, vol. 102, Springer-Verlag, Berlin, 2002, p. 47.
[5] S. Vepřek, S. Reiprich, Thin Solid Films 268 (1995) 64.
[6] H.-D. Männling, D.S. Patil, K. Moto, M. Jilek, S. Vepřek, Surf. Coat. Technol. 146 (147) (2001) 263.
[7] S. Vepřek, M.G.J. Vepřek-Heijman, P. Karvankova, J. Prochazka, Thin Solid Films 476 (2005) 1.
[8] D.V. Shtansky, E.A. Levashov, A.N. Sheveiko, J.J. Moore, J. Mater. Synth. Proc. 6 (1998) 61.
[9] Y. Guo, S. Ma, K. Xu, T. Bell, X. Li, H. Dong, J. Mater. Res. 23 (2008) 2420.
[10] R. Wei, Surf. Coat. Technol. 203 (2008) 538.
[11] M. Dayan, M. Shengli, K. Xu, Surf. Coat. Technol. 200 (2005) 382.
[12] J.-H. Jeon, S.R. Choi, W.S. Chung, K.H. Kim, Surf. Coat. Technol. 188 (189) (2004) 415.
[13] S.L. Ma, D.Y. Ma, Y. Guo, B. Xu, G.Z. Wu, K.W. Xu, P.K. Chu, Acta Mater. 55 (2007) 6350.
[14] G.S. Wu, S.L. Ma, Surf. Eng. 26 (2010) 50.
[15] H. Xu, X. Nie, R. Wie, Surf. Coat. Technol. 201 (2006) 4236.
[16] D.V. Shtansky, Ph.V. Kiryukhantsev-Korneev, I.A. Bashkova, A.N. Sheveiko, E.A. Levashov, Int. J. Refract. Met. Hard Mater. 28 (2010) 32.
[17] L. Donohue, I.J. Smith, W.-D. Münz, I. Petrov, J.E. Greene, Surf. Coat. Technol. 94 (95) (1997) 226.
[18] E. Pflüger, A. Schröer, P. Voumard, L. Donohue, W.-D. Münz, Surf. Coat. Technol. 115 (1999) 17.
[19] F.V. Kiryukhantsev-Korneev, D.V. Shtansky, M.I. Petrzhik, E.A. Levashov, B.N. Mavrin, Surf. Coat. Technol. 201 (2007) 6143.
[20] D.V. Shtansky, Ph.V. Kiryukhantsev-Korneev, A.N. Sheveyko, B.N. Mavrin, C. Rojas, A. Fernandez, E.A. Levashov, Surf. Coat. Technol. 203 (2009) 3595.
[21] D.V. Shtansky, Ph.V. Kiryukhantsev-Korneev, A.N. Sheveiko, A.E. Kutyrev, E.A. Levashov, Surf. Coat. Technol. 202 (2007) 861.
[22] Levashov, A.S. Rogachev, V.I. Ukhvid, I.P. Borovinskaya, Physico-Chemical and Technological Bases of Self-Propagating High-Temperature Synthesis, Binom, Moscow, 1999, p. 134, (in Russian).
[23] D.V. Shtansky, A.N. Sheveyko, D.I. Sorokin, L.C. Lev, B.N. Mavrin, Ph.V. Kiryukhantsev-Korneev, Surf. Coat. Technol. 202 (2008) 5953.
[24] A.A. Galuska, J.C. Uht, N.J. Marguez, J. Vac. Sci. Technol. A 6 (1988) 110.
[25] B.M. Biwer, S.L. Bernasek, J. Electron Spectrosc. Relat. Phenom. 40 (1986) 339.
[26] A. Rizzo, M.A. Signore, L. Mirenghi, T. Di Luccio, Thin Solid Films 517 (2009) 5956.
[27] Handbook of X-ray Photoelectron Spectroscopy, Perkin–Elmer Corporation Physical Electronics Division, 1992.
[28] Y. Lin, P.R. Munroe, Thin Solid Films 517 (2009) 4862.
[29] J. Chastain, R.C. King Jr., Handbook of XPS, Physical Electronics, Eden Prairie, MN, 1992.
[30] A.R. Chourasis, Surf. Sci. Spectra 8 (2001) 45.
[31] F. Schuster, F. Maury, J.F. Nowak, C. Bernard, Surf. Coat. Technol. 46 (1991) 275.
[32] A. Vyas, Y.G. Shen, Z.F. Zhou, K.Y. Li, Compos. Sci. Technol. 68 (2008) 2922.
[33] S. Gredelj, A.R. Gerson, S. Kumar, G.P. Cavallaro, Appl. Surf. Sci. 174 (2001) 240.
[34] G.J. Wan, P. Yang, R.K.Y. Fu, Y.F. Mei, T. Qiu, S.C.H. Kwok, J.P.Y. Ho, N. Huang, X.L. Wu, P.K. Chu, Diamond Relat. Mater. 15 (2006) 1276.
[35] H.C. Barshilia, K.S. Rajarn, J. Mater. Res. 19 (2004) 3196.
[36] L. Escobar-Alarcon, E. Camps, S. Romero, S. Muhl, I. Camps, E. Haro-Poniatowski, Appl. Phys. A 101 (2010) 771.
[37] I. Dreiling, A. Haug, H. Holzschuh, T. Chasse, Surf. Coat. Technol. 204 (2009) 1008.
[38] W. Spengler, R. Kaiser, A.N. Christensen, G. Müller-Vogt, Phys. Rev. B 17 (1978) 17.
[39] P.H. Mayrhofer, , In book:, in: A.A. Voevodin, D.V. Shtansky, E.A. Levashov, J.J. Moore (Eds.), Nanostructured Thin Films and Nanodispersion Strengthened Coatings, NATO Series, Kluwert Acad. Publ, 2004, p. 57.
[40] H. Ezura, K. Ichijo, H. Hasegawa, K. Yamamoto, A. Hotta, T. Suzuki, Vacuum 82 (2008) 476.
[41] S. Veprek, H.-D. Männling, M. Jilek, P. Holubar, Mater. Sci. Eng. A 366 (2004) 202.
[42] P. Karvankova, A. Karimi, O. Coddet, T. Cselle, M. Morstein, Mater. Res. Soc. Symp. Proc. 890 (2006) 0890-Y08-18.1.
[43] K. Yamamoto, T. Sato, K. Takahara, K. Hanaguri, Surf. Coat. Technol. 174 (175) (2003) 620.
[44] G.S. Fox-Rabinovich, K. Yamomoto, S.C. Veldhuis, A.I. Kovalev, G.K. Dosbaeva, Surf. Coat. Technol. 200 (2005) 1804.
[45] S. Imamura, H. Fukui, A. Shibata, N. Omori, M. Setoyama, Surf. Coat. Technol. 202 (2007) 820.